Automotive Experiences
Vol. 9 No. 2 (2026) pp. 644-660
p-ISSN: 2615-6202 e-ISSN: 2615-6636

Research Paper

Toward Diesel-Range Fuel Properties: Catalytic Upgrading of Waste Cooking Oil Biodiesel over Acid-Activated Bentonite

Muhammad Latifur Rochman[1,2], **Nurkholis Hamidi**[1], **Winarto**[1]

[1]Department of Mechanical Engineering, Universitas Brawijaya, Malang 65145, Indonesia
[2]Center of Energy for Society and Industry, Universitas Muhammadiyah Magelang, Magelang 56172, Indonesia

hamidy@ub.ac.id

https://doi.org/10.31603/ae.15630

Published by Automotive Laboratory of Universitas Muhammadiyah Magelang

Article Info
Submitted:
15/12/2025
Revised:
25/08/2026
Accepted:
25/08/2026
Online first:
25/08/2026

Abstract

Waste cooking oil (WCO)-derived biodiesel represents a promising renewable fuel because it simultaneously supports waste valorization, reduces dependence on petroleum-derived diesel, and lowers feedstock costs. However, its relatively high viscosity, oxygenated ester structure, and lower energy density compared with conventional diesel can limit its fuel performance. Most existing upgrading strategies address these limitations through catalytic cracking or deoxygenation at temperatures above 250–350 °C, frequently involving pressurized hydrogen and extensive conversion of fatty acid methyl esters (FAME) into hydrocarbon-rich fuels, leaving limited understanding of whether biodiesel properties can instead be improved through low-severity treatment while preserving its FAME-rich character. This study investigated H_2-free mild catalytic upgrading of WCO-derived biodiesel using untreated bentonite and HCl-activated bentonite at catalyst loadings of 0.20, 0.40, 0.60, and 0.80 wt% in a rotary reactor operated at 150 °C for 1 h, followed by density, kinematic viscosity, calorific value, flash point, FTIR, and GC–MS analyses. The treatment caused only negligible variation in density, from 0.842 g/cm³ for the initial biodiesel to 0.843–0.844 g/cm³ after upgrading, indicating that the bulk molecular characteristics of the fuel were largely retained, while the kinematic viscosity decreased substantially from 4.94 cSt to minimum values of 3.54 and 3.55 cSt at 0.20 and 0.40 wt%, respectively. The calorific value increased from 41.46 MJ/kg to a maximum of 42.39 MJ/kg at 0.80 wt%, corresponding to an improvement of approximately 2.24%, while the 0.60 and 0.80 wt% samples exhibited flash points of 57.5 and 56.5 °C, respectively. GC–MS analysis revealed a compositional redistribution from 65.48% FAME and 16.13% aliphatic hydrocarbons in the initial biodiesel to approximately 53.46% FAME and 28.48% aliphatic hydrocarbons at 0.80 wt%; meanwhile, the 0.40 wt% sample showed the formation of approximately 3.80% C12 hydrocarbons, consistent with its lower viscosity and greater volatility. FTIR spectra retained the characteristic ester C=O and long-chain aliphatic bands, supporting limited molecular transformation rather than extensive destruction of the FAME framework. These findings demonstrate that low-temperature, low-catalyst-loading bentonite treatment can selectively redistribute biodiesel components and tune fuel properties without deep conversion, providing a low-severity upgrading pathway that bridges conventional biodiesel processing and high-temperature hydrocarbon-fuel production.

Keywords: Biodiesel; Waste cooking oil; Catalytic upgrading

1. Introduction

Rising global energy demand and growing concerns about environmental impacts have intensified research into renewable and sustainable energy sources. In this context, biodiesel has emerged as a promising alternative to fossil-based fuels [1]. Among various feedstocks, waste cooking oil (WCO) is a preferred option due to its relatively low cost and

environmental benefits. The use of WCO not only reduces production costs by 60–70% compared to vegetable oils [2], [3], [4], but also helps mitigate waste disposal issues and environmental pollution [5], [6], [7], [8]. WCO can be converted into fatty acid methyl esters (FAME) through a transesterification process [7], [8]. However, the variability in WCO composition, which is influenced by the type of food fried, cooking temperature, and the frequency of oil reuse significantly affects free fatty acid (FFA) content, catalyst stability, and overall conversion efficiency [9], [10]. This variability is consistent with previous reports showing that the physicochemical characteristics of WCO and the resulting biodiesel are strongly dependent on feedstock origin, frying conditions, water and impurity contents, and processing conditions [7].

Biodiesel has different physicochemical properties compared to diesel fuel. According to ASTM D6751 and EN 14214 standards, the kinematic viscosity, density, and flash point of biodiesel typically range from 4.5–5.0 cSt, 860–900 kg/m³, and 120–170 °C. In contrast, diesel fuel as defined by ASTM D975, has viscosity, density, and flash point values of 1.9–4.1 cSt, 820–860 kg/m³, and 52–96 °C. This comparison shows that biodiesel generally has higher viscosity and flash point than petrodiesel, resulting in differences in atomization, combustion behavior, and cold-flow performance [7], [11]. Milano *et al*. [12] investigated the production of biodiesel from waste cooking oil (WCO) via transesterification using potassium hydroxide (KOH) as a catalyst. The results showed a kinematic viscosity of 5.01 cSt at 40 °C, a density of 862.1 kg/m³ at 15 °C, and a flash point of 154 °C. Although the density and flash point met the ASTM D6751 and EN 14214 biodiesel specifications, the viscosity exceeded the upper limit, indicating less-than-optimal flow and atomization characteristics compared to diesel fuel.

Similarly, Nguyen *et al*. [13] conducted a comparative review of biodiesel properties and reported that WCO-based biodiesel exhibited a density of 890 kg/m³, a kinematic viscosity of 4.36 cSt, and a flash point of 175.4 °C, further highlighting its deviation from the physicochemical characteristics of diesel fuel. In another study, Demir *et al*. [14] synthesized biodiesel from WCO using a deep eutectic solvent (DES) catalyst consisting of p-toluenesulfonic acid monohydrate (PTSA) and tetraethylammonium bromide (TEAB) in a 1:1 molar ratio. The resulting biodiesel exhibited a density of 890 kg/m³, a viscosity of 5.5 cSt, and a flash point of 160 °C, indicating that the biodiesel still failed to meet the desired range for diesel fuel. More recently, Karthikeyan *et al*. [15] investigated the transesterification of WCO using a $BaZrO_3$ catalyst and reported density and viscosity values ranging from 880–900 kg/m³ and 4.5–6.0 cSt, respectively. Although data on calorific value and flash point were not provided, the measured properties still fall outside the specifications for diesel fuel. Collectively, these studies reinforce the finding that biodiesel derived from WCO generally has higher viscosity and density compared to petrodiesel, which can adversely affect atomization, fuel injection, and overall engine performance in compression-ignition systems [7].

These limitations indicate that further improvements are needed to bring WCO biodiesel closer to the characteristics of petrodiesel. In particular, the presence of oxygenated ester structures in biodiesel contributes to differences in heating value, oxidation stability, and cold-flow behavior compared with hydrocarbon diesel [7], [11], [16]. Previous studies have consequently devoted considerable attention to catalyst development, particularly heterogeneous catalysts, because of their easier separation, potential recyclability, reduced wastewater generation, and ability to improve the efficiency of biodiesel conversion processes [8], [16], [17]. Therefore, enhancing catalytic performance has become a crucial step toward improving the quality and acceptance of biodiesel-derived fuels.

2. Literature Review

Research on the upgrading of lipid-based fuels since 2020 has shown strong progress toward the production of hydrocarbon fuels that increasingly resemble conventional diesel and jet fuels. Results from previous studies indicate that emerging approaches can be grouped into three main categories: partial deoxygenation, catalytic cracking accompanied by deoxygenation, and deep conversion of FAME, triglycerides, and fatty acids into hydrocarbon-rich fuels. Although temperatures around 250–300 °C are sometimes

described as mild conditions compared to conventional hydrothermal or pyrolysis processes, nearly all of these studies still employ conditions that are significantly harsher than the 150 °C temperature used in this study.

The partial deoxygenation approach provides a conceptual basis that oxygen removal does not have to be complete to improve fuel characteristics. In the pyrolysis of *Isochrysis sp.*, a fly ash-based Li–Na catalyst reduced the oxygen content of the bio-oil by approximately 25 wt.% while simultaneously increasing the formation of paraffins and olefins. However, that process was still conducted at 500 °C; thus, the term partial refers to the degree of oxygen removal, not to low reaction severity [18]. Similarly, the conversion of palmitic acid using layered alkali titanate yields approximately 47% hydrocarbons and is equivalent to about an 80% reduction in oxygen content, but requires temperatures up to 400 °C [19]. Thus, the literature indicates that partial deoxygenation has been developed as a concept but has not yet been widely applied within the framework of low-temperature upgrading of FAME, which is intentionally retained as the primary fuel component.

Studies using acid catalysts and porous materials show that increasing cracking activity can accelerate hydrocarbon formation but simultaneously increases the risk of over-conversion. Chainlike ZSM-5, with a mesoporous structure and moderate acidity, for example, yields a light olefin selectivity of 75.7% from the cracking of oleic acid at 400 °C [20]. Meanwhile, $NbOPO_4$ is capable of integrating deoxygenation, cracking, and partial isomerization of vegetable oil at 350 °C and 10 bar N_2, yielding a conversion of up to 95% and fractions falling within the gasoline, SAF, and green diesel ranges [21]. These results demonstrate the benefits of acid catalysts but also indicate that current strategies are generally aimed at extensively breaking down lipid structures rather than making limited modifications to FAME feedstock.

Another notable trend is the development of H_2-free deoxygenation processes to reduce reliance on external hydrogen. Ni/MgO–Al_2O_3 in the deoxygenation of oleic acid yielded a hydrocarbon content of up to 95.12%, with 75.90% of the product falling into the category classified as green diesel like fuel [22]. Dolomite in the pyrolysis of used cooking oil yields 68.06% bio-oil with a selectivity of 57.27% toward gasoline- and diesel-range hydrocarbons, but requires a temperature of 450 °C and 6 wt.% catalyst [23]. A recent study on palm fatty acid distillate using Ni, Co, and NiCo supported on kaolin-derived zeolites was able to produce 77–83% C_8–C_{17} hydrocarbons without external hydrogen at 250–350 °C [24]. Furthermore, the integration of cracking and in situ hydrogenation of used cooking oil can yield approximately 80.22% SAF at 350 °C with only 0.5 wt.% Ni/Al_2O_3. However, this system still relies on in situ hydrogen generation to drive hydrodeoxygenation [25].

Although the H_2-free process reduces one of the main contributors to process severity, the operating temperature generally remains between 250 and 500 °C. These conditions promote simultaneous decarboxylation, decarbonylation, cracking, aromatization, and secondary reactions. On a Pt/CeO_2 catalyst, for example, the deoxygenation of stearic acid yields an olefin selectivity of approximately 41%, indicating that the combination of metal sites and oxygen vacancies can direct the decarbonylation pathway toward hydrocarbon formation [26]. Further mechanistic studies on Ni surfaces show that the adsorption geometry of carboxylic acids plays a direct role in the decarbonylation pathway, confirming that feedstock–surface interactions are a determining factor in oxygen elimination [27]. These findings are relevant for understanding the function of catalytic sites, but the conditions that produce such deep deoxygenation are not identical to those required to preserve most of the FAME structure.

Conversely, the use of external H_2 enables very high deoxygenation at relatively lower temperatures compared to thermal cracking, but increases the complexity of the system. NiCu/Mo–$NbOPO_4$ yields up to 84.16% selectivity for C_{18} from oleic acid at 250 °C, but requires 3 MPa of H_2 and a reaction time of 7 hours [28]. Ni supported on schungite yields nearly 100% C_{10}–C_{18} alkanes at 280 °C with a partial pressure of H_2 of 1.5 MPa [29]. Hydroprocessing of camelina oil results in the complete conversion of triacylglycerides to hydrocarbons at approximately 360 °C and 50 bar H_2 [30], while the selective deoxygenation of palm oil using Ni/CeO_2–ZrO_2 maintains triglyceride conversion above 85% and a C_{15}–C_{18} yield above

80% at 300 °C [31]. Recent optimization of palm stearin using Ni/ZrO_2 even achieved a 97.92% conversion and an 87.75% green diesel yield at 350 °C and 34 bar H_2 [32].

The difference between established approaches and this study becomes most evident when FAME is used directly as a feedstock. A study using MnFeCoNiCu/C converted FAME at 350 °C and 2 MPa H_2, achieving 100% FAME conversion, with a selectivity of 48.35% toward bio-jet fuel and 51.05% toward green diesel [33]. Another study using methyl oleate along with vegetable oil also employed temperatures of 300–340 °C and pressures around 2 MPa to drive hydrodeoxygenation via Pt/Pd, NiMo, and zeolite–alumina systems [34]. Both studies demonstrate that FAME and fatty acid esters can be used as precursors for hydrocarbon fuels; however, the objective of the reaction is to eliminate the FAME identity through deep conversion, rather than to enhance the properties of FAME by retaining most of the original ester.

A single-step approach at lower temperatures has also been developed. TiO_2 modified with Ru/C was able to integrate deoxygenation and cracking at 260 °C and yielded 35.2 wt.% jet-range alkanes from oleic acid [35]. Catalytic pyrolysis of microalgal lipids using hierarchical HZSM-5 modified with ZnO, La_2O_3, or CeO_2 increases the hydrocarbon content and kerosene fraction to over 40%, but the mechanism still involves decarboxylation, decarbonylation, cracking, and aromatization [36].

The summary in **Table 1** shows that most available technologies are designed to convert as many lipids, fatty acids, triglycerides, or FAME as possible into hydrocarbons, so that the final product can be used as green diesel or sustainable aviation fuel. Even mild processes generally still take place at 250–350 °C, while cracking and deoxygenation without H_2 are often carried out at 350–500 °C. Studies that directly use FAME have even reported up to 100% conversion at 350 °C and 2 MPa H_2, meaning the initial FAME is almost entirely converted into hydrocarbon-rich fuel. This approach essentially treats biodiesel or lipids as feedstocks that must be reprocessed in an upgrading unit before use, rather than as fuels whose properties can be improved through simple catalytic treatment. Based on previous study, the use of a temperature of 150 °C in this study is intended to explore whether commercially available FAME biodiesel can undergo mild catalytic upgrading with a minimum level of transformation. This would allow its characteristics to be shifted closer to those of conventional diesel without resorting to hydrodeoxygenation or high-temperature catalytic cracking

3. Material and Methods

3.1. Material

The materials used in this study included sodium bentonite (Na-bentonite), hydrochloric acid (HCl, 37%), and biodiesel derived from waste cooking oil (WCO-biodiesel). The Na-bentonite served as the base catalyst material, while HCl was employed as the activating agent to modify the surface properties of the bentonite through acid treatment. The WCO-biodiesel used in this study was previously produced via transesterification.

3.2. Catalyst Activation

The activation of Na-bentonite was carried out by mixing the clay with an aqueous HCl solution at a ratio of 1:11.75 (w/v) to promote proton exchange and partial removal of exchangeable cations and impurities while minimizing excessive structural degradation of the bentonite framework, in accordance with commonly reported acid-activation conditions for smectite clays [37]. The mixture was continuously stirred using a magnetic hotplate stirrer at 100 °C for 3 h to enhance ion exchange and acid treatment efficiency without causing severe collapse of the layered clay structure during the wet activation step. After activation, the sample was repeatedly washed with distilled water, then dried and calcined.

3.3. Mild Catalytic Upgrading Process

Mild catalytic upgrading experiments were conducted using untreated catalyst (B) was tested at a concentration of 0.2 wt%, while the treated catalysts was evaluated at concentrations of 0.2, 0.4, 0.6, and 0.8 wt% relative to the mass of biodiesel. The reactions were conducted in a rotary reactor, which allowed continuous rotation to ensure uniform mixing and improved heat exposure between the catalyst and feedstock. Heat transfer in this system occurred primarily via

Table 1. Previous study

Feedstock	Catalyst	Reaction Temp.	H_2	Reaction Severity	Final Fuel Class	Limitations	Ref.
Waste cooking oil	Ni/Al_2O_3	350 °C	H_2 formed *in situ*	SAF yield 80.22%	Hydrocarbon-rich SAF	Still uses 350 °C and in situ hydrogenation	[25]
Microalgae bio-oil	Li–Na fly ash	500 °C	No	O decrease ±25 wt.%	Partially deoxygenated oxygenate/hydrocarbon mixture	Partial deoxygenation, but at pyrolytic temperatures	[18]
Oleic acid	NiCu/Mo–$NbOPO_4$	250 °C	Yes	C_{18} selectivity 84.16%; % O removal not reported	Hydrocarbon-rich	Higher temperature, high H_2 pressure, and extended duration	[28]
Palm fatty acid distillate	Ni/Co/NiCo–zeolite	250–350 °C	Tidak	77–83% C_8–C_{17} hydrocarbons	Hydrocarbon-rich green diesel	Hydrocarbon-rich green diesel H_2-free, but with much higher metal loading and temperatures	[24]
Microalgal lipids	Metal-oxide-modified hierarchical HZSM-5	350 °C	No	Oxygenates decrease; kerosene fraction >40%; % deoxygenation not reported	Hydrocarbon/kerosene-rich	Cracking and aromatization are the dominant pathways	[36]
Camelina oil	NiMoP/γ-Al_2O_3 and NiMoCuP/ZrO_2–γ-Al_2O_3	340–370 °C	Yes	Complete TAG conversion under certain condition	Hydrocarbon-rich diesel components	Requires high-pressure H_2 and deep conversion	[30]
FAME	MnFeCoNiCu/C	350 °C	Yes	100% FAME conversion	Hydrocarbon-rich: 48.35% bio-jet + 51.05% green diesel	Direct comparison; completely removes FAME	[33]
Palmitic acid	Layered alkali titanate	≤400 °C	No	±80% oxygen reduction; ±47% hydrocarbon yield	Partially deoxygenated/hydrocarbon-enriched	Partial deoxygenation but at high temperatures	[19]
Oleic acid	Ni/MgO–Al_2O_3	450-500 °C	No	HC 95.12%; green diesel 75.90% in 10% Ni	Hydrocarbon-rich green diesel-like	High metal loading and deep conversion target	[22]
Stearic acid	Ni/schungite	280 °C	Yes	Almost 100% C_{10}–C_{18} alkanes	Hydrocarbon-rich	H_2 and supercritical solvent required	[29]
Vegetable oils	$NbOPO_4$	350 °C	No	Conversion until 95%	Hydrocarbon-rich gasoline/SAF/green diesel	Extensive acid-catalyzed cracking and deoxygenation	[21]
Vegetable oil and methyl oleate	Pt/Pd/zeolite–Al_2O_3, NiMo/Al_2O_3, Pd/C	300–340 °C	Yes	Conversion until 99%	Hydrocarbon-rich renewable diesel	Esters are converted via hydrogenation/hydrogenolysis	[34]
Waste cooking oil	Dolomite	450 °C	No	57.27% selectivity for gasoline and diesel hydrocarbons	Hydrocarbon-rich bio-oil	High temperature and catalyst loading	[23]
Oleic acid	Chainlike ZSM-5	400 °C	No	Oleic-acid cracking; 75.7% light olefin selectivity	Light-hydrocarbon-rich	Cracking is too intensive for FAME-preserving upgrading	[20]
Palm oil	Ni/ZrO_2 and Ni/CeO_2–ZrO_2	300 °C	Yes	TG conversion >85%; C_{15}–C_{18} yield >80%	Hydrocarbon-rich green diesel	Deep deoxygenation with Ni/H_2	[31]
Oleic acid, triglyceride, vegetable oil	TiO_2-modified Ru/C	260 °C	Yes	Jet-range alkane carbon yield 35.2 wt.%	Hydrocarbon-rich bio-jet	Using precious metals and a solvent system	[35]

Feedstock	Catalyst	Reaction Temp.	H_2	Reaction Severity	Final Fuel Class	Limitations	Ref.
Stearic acid	Pt/CeO_2, Pt/ZrO_2, Pt/Fe_2O_3	380-405 °C	H_2 formed *in situ*	Pt/CeO_2 olefin selectivity 41%	Hydrocarbon/olefin-rich	Requires Pt and is geared toward deep decarbonylation	[26]
Palm stearin	Ni/ZrO_2	350 °C	Yes	Conversion 97.92%; green diesel yield 87.75%	Hydrocarbon-rich green diesel	Nearly complete conversion and requires pressurized H_2	[32]
WCO Biodiesel	Bentonit and HCl-activated bentonite	150 °C	No	-	Diesel-like fuel	Explores the low-temperature/low-loading region not covered by the studies above	This research

conduction from the chamber to the reactor wall, followed by internal convective mixing induced by rotational motion. The reactor temperature was maintained at 150 °C for a total reaction time of 1 h. The actual feedstock temperature was monitored every 15 min, with measured values of 70, 84, 98, and 104 °C at respective intervals, indicating operation under mild liquid-phase conditions rather than conventional high-temperature thermal cracking. After completion, the reaction products were cooled to room temperature and filtered to separate the catalyst residues.

3.4. *Product Characterization*

The liquid products obtained after catalytic upgrading were analyzed for their physicochemical properties, including kinematic viscosity, density, calorific value, and flash point. The chemical functional groups of the treated biodiesel were identified using Fourier Transform Infrared Spectroscopy (FTIR), while the detailed hydrocarbon composition and distribution were determined using Gas Chromatography–Mass Spectrometry (GC–MS). These analyses were performed to evaluate the effect of catalyst treatment and concentration on the quality and composition.

4. Results and Discussion

4.1. *Density*

Figure 1 presents the density values of WCO-biodiesel, untreated bentonite (B), and biodiesel samples obtained through mild catalytic upgrading using different catalyst concentrations (0.20%, 0.40%, 0.60%, and 0.80%). The density of raw WCO was 0.842 g/cm³, which slightly increased to 0.843 g/cm³ after treatment with untreated bentonite. Similar values (0.843 g/cm³) were observed for biodiesel processed at 0.20%, 0.40%, and 0.60% catalyst loadings, while the highest density of 0.844 g/cm³ was obtained at 0.80%.

The very small variation in density (within ±0.002 g/cm³) indicates that the treatment under the present conditions did not induce significant molecular restructuring. This observation is consistent with the relatively low operating temperature (150 °C), which is insufficient to promote extensive bond cleavage or deep compositional changes typically associated with high-temperature cracking processes. Therefore, the bulk molecular composition of the biodiesel remains largely preserved.

From a molecular perspective, density is strongly influenced by the presence of oxygenated compounds and the polarizability of molecules. WCO-biodiesel primarily consists of fatty acid methyl esters (FAME), which contain polar functional groups such as ester (–COO–) moieties [38]. These groups contribute to higher intermolecular interactions through dipole–dipole forces, leading to relatively higher densities compared to non-polar hydrocarbon fuels. Since the upgrading conditions applied in this study are mild, the oxygenate fraction is expected to remain largely unchanged, resulting in minimal variation in density across all catalyst loadings.

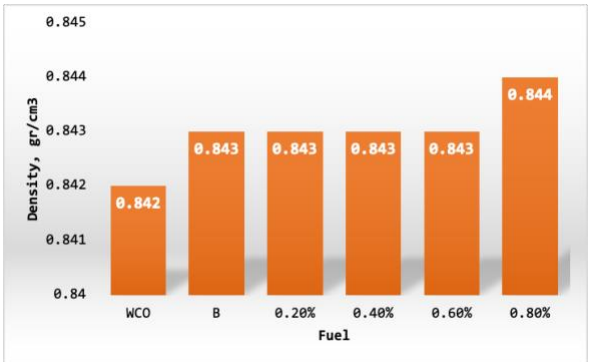

Figure 1. Density value

When compared to the ASTM D975 specification for petrodiesel (0.820–0.860 g/cm³), all upgraded biodiesel samples fall within the acceptable range. Previous studies have reported that conventional biodiesel exhibits higher densities (0.880–0.920 g/cm³) due to its oxygenated nature [39]. The relatively lower density observed in this study indicates that the biodiesel is already within a suitable range for fuel applications, even without extensive structural transformation.

4.2. *Kinematic Viscosity*

After establishing the density behavior, the variation in kinematic viscosity offers further insights into the fuel's flow characteristics (**Figure 2**). The WCO-biodiesel exhibited the highest viscosity of 4.94 cSt, consistent with the presence of long-chain triglycerides and oxygenated residues that increase molecular weight. Treatment with sample B reduced viscosity to 3.80 cSt, suggesting partial adsorption or cracking of heavier molecular species on the bentonite surface.

The most significant viscosity reduction occurred at 0.20% and 0.40% catalyst loadings, yielding 3.54 cSt and 3.55 cSt, respectively. These findings confirm that HCl-activated bentonite effectively catalyzed the cleavage of high molecular weight triglycerides into lighter hydrocarbons, improving fluidity and reducing internal friction. However, at higher catalyst concentrations (0.60% = 4.82 cSt and 0.80% = 4.50 cSt), viscosity increased again. This increase may be associated with secondary reactions such as oligomerization or the formation of heavier intermediates under higher catalyst loading. This nonlinear correlation between catalyst dosage and viscosity has been widely reported in heterogeneous acid catalysis, where excessive catalyst loading induces diffusion limitations and secondary reactions [40].

According to ASTM D975, diesel fuels should have viscosities between 1.9–4.1 cSt at 40 °C. Feedstock obtained with 0.20% and 0.40% catalyst loadings meets this specification, while higher loadings slightly exceed the upper limit. Since dynamic viscosity (η) is the product of kinematic viscosity (ν) and density (ϱ), the observed decrease in ν also implies lower η, facilitating better atomization and air–fuel mixing. Lower viscosity enhances spray breakup and combustion efficiency, contributing to smoother engine operation and reduced emissions. These observations align with reports by Yadav *et al.* [41], who noted that catalytic upgrading and optimized transesterification can significantly improve biodiesel rheology without sacrificing energy density.

4.3. *Calorific Value*

The calorific value, as shown in **Figure 3**, indicates that WCO-biodiesel has a calorific value of 41.46 MJ/kg, while all products after upgrading treatment range from 41.59 to 42.39 MJ/kg. The highest value was obtained with a catalyst concentration of 0.80 wt%, namely 42.39 MJ/kg, representing an increase of approximately 2.24% compared to the initial feedstock. Although the absolute increase is not large, this trend is significant because the process was carried out under relatively mild conditions. The response of the calorific value to catalyst concentration exhibits a nonlinear pattern. After rising to 42.10 MJ/kg with the untreated catalyst (B), the calorific value decreased slightly at concentrations of 0.20 and 0.40 wt%, then increased again at 0.60 wt% and reached a maximum at 0.80 wt%. At low to moderate catalyst concentrations, the partial transformation of FAME can produce a mixture of compounds with energy characteristics not significantly different from those of the feedstock. Conversely, at higher concentrations, greater contact between fuel molecules and active catalyst sites enhances the formation of fractions with lower oxygen content or higher proportions of C–H and C–C bonds, thereby contributing positively to the calorific value [42].

Interestingly, the increase in maximum calorific value is only about 0.93 MJ/kg compared

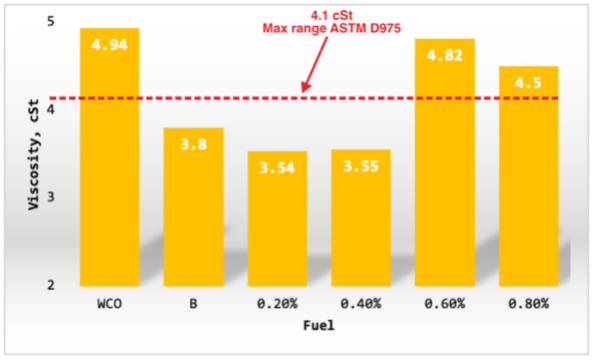

Figure 2. Kinematic viscosity value

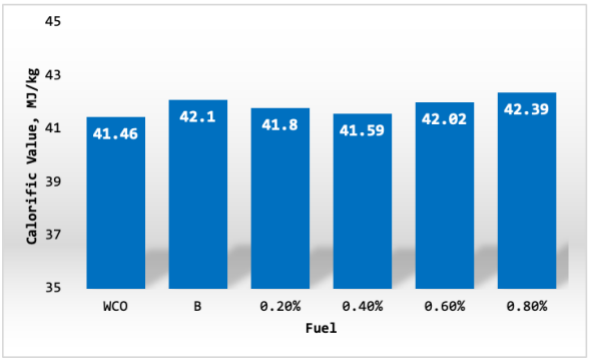

Figure 3. Calorific value

to the initial feedstock. This limited magnitude of change is consistent with the nature of the process, which was developed as mild upgrading rather than deep deoxygenation. In conventional deoxygenation processes at much higher temperatures, extensive oxygen removal via decarboxylation, decarbonylation, or hydrodeoxygenation can transform FAME-rich fuel into a hydrocarbon mixture that is chemically very different from the original biodiesel [43]. In contrast, under mild conditions, the main structure of FAME is likely retained, while only some components undergo transformation. The highest value at a concentration of 0.80 wt% also suggests a possible shift in product composition toward a more energetically favorable state. However, the calorific value alone is not sufficient to conclude that this increase is exclusively due to deoxygenation. The formation of non-FAME compounds, changes in carbon chain length distribution, changes in saturation levels, and an increase in the aromatic fraction may all contribute to the final calorific value.

4.4. Flashpoint

Figure 4 presents the flash point values of WCO, unactivated bentonite, and cracked feedstock samples. The flash point of raw WCO was 56.5 °C, slightly increasing to 58.5 °C after treatment with unactivated bentonite due to the removal of volatile impurities. Conversely, cracked feedstock samples at 0.20% and 0.40% catalyst loadings exhibited lower flash points (50 °C and 52 °C), indicating increased volatility caused by the formation of lighter hydrocarbons. At higher catalyst loadings (0.60% and 0.80%), flash points rise again to 57.5 °C and 56.5 °C, respectively, implying the formation of heavier, more stable compounds via condensation or recombination reactions. Among the tested conditions, the 0.60% catalyst sample showed the most favorable balance between calorific value and flash point within the present experimental window.

According to ASTM D975, diesel fuel should have a flash point of at least 52 °C. Based on this criterion, the 0.20% sample (50 °C) does not satisfy the ASTM D975 threshold, the 0.40% sample lies at the lower compliance boundary, and the 0.60% and 0.80% samples fall within the diesel flash-point range. In particular, the lower flash point of the 0.20% sample suggests a higher proportion of volatile components and may imply greater handling, storage, and transportation concerns than the other upgraded products. The observed variation aligns with the findings of Fu [44], who demonstrated that oxygenated biodiesels exhibit higher flash points due to reduced vapor pressure, while inclusion of lighter hydrocarbons lowers it [45]. The results herein thus confirm that the cracked WCO biodiesel possesses sufficient ignition stability and handling safety comparable to commercial diesel.

4.5. FTIR Analysis

FTIR spectroscopy is widely used as a rapid, non-destructive tool to confirm biodiesel functional groups and to support quality monitoring, especially for complex matrices such as waste cooking oil (WCO) where overlapping signals and feedstock variability can occur [46]. For WCO-derived biodiesel, the most diagnostic mid-IR regions typically include the ester carbonyl band near ~1745 cm^{-1}, the aliphatic C–H stretching bands near ~2923 and ~2853 cm^{-1}, and the C–O region where a relatively interference-minimized methyl-ester marker has been reported around ~1195 cm^{-1} [47].

Figure 4. Flashpoint

In this work, FTIR spectra were recorded (4000–600 cm^{-1}, 4 cm^{-1} resolution, 24 scans). The evaluated samples were: WCO, B, and catalytic upgrading with HCl-activated bentonite at 0.40% and 0.80%. Across all samples, the FTIR peak positions display a highly consistent functional-group profile dominated by long-chain aliphatic structures and ester functionalities. The WCO spectrum exhibits characteristic bands at 2922.06 and 2853.10 cm^{-1} (aliphatic $–CH_2$ stretching), a strong band at 1744.55 cm^{-1} (ester C=O stretching), and fingerprint bands at 1459.49 ($–CH_2$ bending), 1376.95 ($–CH_3$ bending), 1169.54 (C–O stretching region), and 722.20 cm^{-1} ($(CH_2)_n$ rocking). After catalytic cracking, all products retained the same diagnostic bands with very small wavenumber differences.

The highly similar FTIR profiles indicate that catalytic treatment did not induce substantial changes in the dominant mid-IR functional groups of the biodiesel. The characteristic ester and aliphatic bands were largely preserved, suggesting that the reaction proceeded without extensive cleavage of the molecular framework or formation of new dominant functionalities. Considering the relatively low reaction temperature, the observed spectral stability is consistent with mild catalytic upgrading, in which limited bond cleavage, surface-mediated interactions, and redistribution of existing components are more likely than extensive cracking or deoxygenation.

Although no pronounced peak shifts were observed, slight variations in the ester C=O stretching region may indicate subtle changes in the local chemical environment of the carbonyl groups. Interactions between biodiesel molecules and active sites on the bentonite surface can modify electron density, polarity, or intermolecular interactions sufficiently to affect band intensity or shape without producing readily distinguishable new functional groups. However, the similarity of the spectra should not be interpreted as evidence of unchanged oxygen content, as FTIR primarily identifies functional-group environments rather than quantitatively determining the extent of oxygen removal. Previous studies have similarly demonstrated the utility of FTIR for identifying major functional groups and monitoring compositional variations in oils and fuels, including acidity/FFA-related changes and compositional deviations [48], [49]. The principal absorption bands and their assignments are summarized in **Table 2**.

This interpretation is further supported by the physicochemical properties. Density remained nearly unchanged across the treatments (0.842–0.844 g/cm^3), whereas viscosity varied more noticeably with catalyst loading. This divergence suggests that the catalytic treatment primarily altered the relative distribution and molecular characteristics of the fuel components rather than causing wholesale transformation of the dominant chemical structure. The corresponding variation in calorific value further indicates compositional redistribution, potentially involving changes in the relative abundance of ester, hydrocarbon-like, and other minor components. Thus, the FTIR results are best interpreted together with the physicochemical and compositional analyses to characterize the extent of mild catalytic upgrading. The overlaid ATR–FTIR spectra of WCO and the catalytically treated samples are presented in **Figure 5**.

4.6. GC–MS Analysis

WCO-biodiesel consists primarily of FAME, which approximately 65.48% of the reported chromatographic area (**Table 3**). Major components include 9-cis,11-trans-octadecadienoic acid methyl ester (15.94%), methyl 13-octadecanoate, appearing as several

Table 2. Major FTIR absorption bands

Band assignment	WCO (cm^{-1})	150B (cm^{-1})	150-1 (cm^{-1})	150-2 (cm^{-1})
$\nu_{as}(CH_2)$ stretching	2922.06	2922.0787	2922.0298	2922.0614
$\nu_{s}(CH_2)$ stretching	2853.1	2853.1066	2853.0404	2853.0964
ν(C=O) ester stretching	1744.55	1744.5607	1744.4344	1744.5497
δ(CH_2) bending/scissoring	1459.49	1459.036	1459.2621	1459.2946
δ(CH_3) bending	1376.95	1376.9403	1376.8985	1376.9371
ν(C–O) stretching (ester region)	1169.54	1169.4871	1169.4503	1169.4846
ϱ($(CH_2)_n$) rocking (long-chain)	722.2	722.1791	722.0578	722.2007

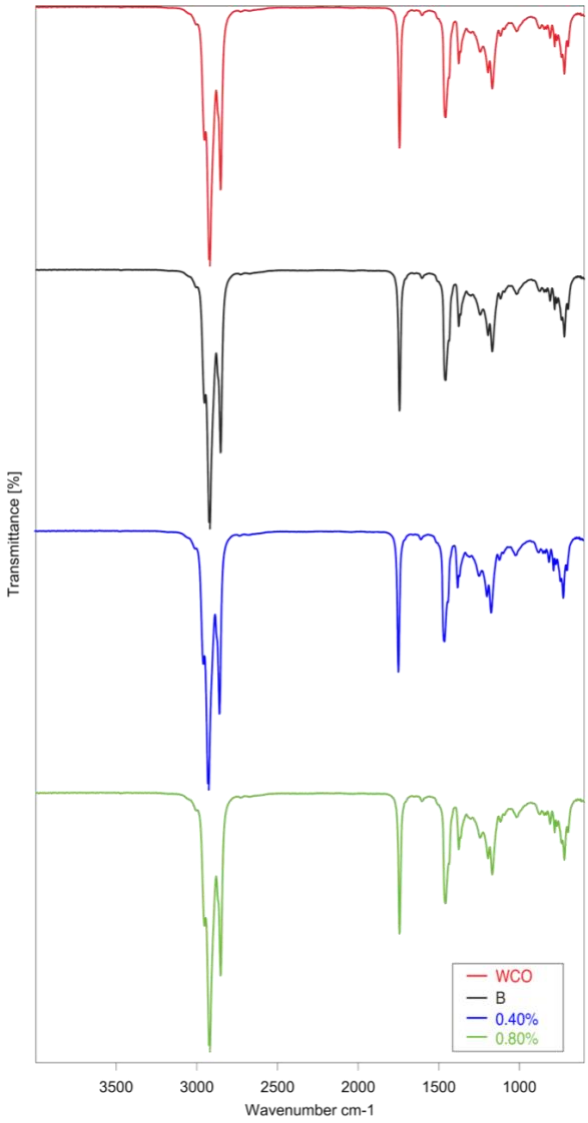

Figure 5. FTIR spectra

chromatographic peaks with a combined area of approximately 23.64%, methyl hexadecanoate (10.46%), methyl stearate (9.53%), and 14-methylpentadecanoic acid, methyl ester (5.91%). In addition to FAME, the initial sample already contained C17–C21 aliphatic hydrocarbons, including heptadecane, octadecane, eicosane, and heneicosane, with a combined area of approximately 16.13%. Aromatic and cyclic compounds were also detected, including mesitylene, benzocycloheptatriene-related compounds, biphenyl derivatives, and substituted azulene.

Process with untreated bentonite (B) resulted in a clear redistribution of the detected compounds as shown in **Table 4**. The total FAME area decreased from 65.48% in WCO biodiesel to approximately 55.13%, while the aliphatic hydrocarbon fraction increased from approximately 16.13% to 24.03%. In particular, a broader distribution of linear hydrocarbons was observed, including hexadecane (C16), heptadecane (C17), octadecane (C18), nonadecane (C19), eicosane (C20), heneicosane (C21), and tetracosane (C24). These changes indicate that even untreated bentonite can influence the product composition, likely through adsorption, surface-mediated bond cleavage, and the redistribution of heavier oxygenated molecules [50]. This interpretation is consistent with the decrease in kinematic viscosity from 4.94 cSt for WCO biodiesel to 3.80 cSt after treatment with B, while simultaneously increasing the calorific value from 41.46 to 42.10 MJ/kg.

A different compositional response was observed at a catalyst loading of 0.40% as following **Table 5**. FAME remained the dominant detectable fraction, indicating that the structure of the ester-based fuel was largely preserved under mild reaction conditions. However, the most distinctive feature of these samples was the appearance of several dodecane (C12) peaks with a combined area of approximately 3.80%, along with C17, C19, and C21 hydrocarbons. The presence of C12 hydrocarbons provides evidence of a greater contribution from carbon chain scission compared to what was observed in the original WCO biodiesel. This shift in composition offers a plausible molecular explanation for the low viscosity of the 0.40% sample (3.55 cSt) and its relatively low flash point of 52 °C. The formation of lower-molecular-weight hydrocarbons reduces intermolecular resistance to flow while increasing volatility. Thus, the very low viscosity in the intermediate catalyst loading is more likely due to a redistribution toward lighter components than to extensive deoxygenation of the entire FAME fraction [41].

At 0.80% (**Table 6**), the compositional profile shifted more distinctly toward a product enriched in aliphatic hydrocarbons. The combined contribution of FAME decreased to approximately 53.46%, while aliphatic hydrocarbons accounted for approximately 28.48% of the total chromatographic area. In addition to linear C16–C24 hydrocarbons, a significant amount of 2,6,10,14-tetramethylpentadecane (5.82%) was detected. Compared to the original WCO biodiesel, the

aliphatic fraction increased by approximately 12.35 percentage points, while the FAME contribution decreased by approximately 12.02 percentage points. Importantly, however, more than half of the detected product remained FAME.

The enrichment of oxygen-free aliphatic compounds at 0.80% is consistent with its higher calorific value. Hydrocarbons contain more C–C and C–H bonds and lack oxygen bound to esters, so their contribution to the fuel's energy density is

Table 3. WCO-biodiesel GC-MS results

Peak	RT	Area (%)	Identified Compounds	Molecular Formula
1	2.374	0.53	Carbonic acid, 2-ethylhexyl nonyl ester	C18H36O3
2	3.187	0.94	Carbonic acid, decyl 2-ethylhexyl ester	C19H38O3
3	6.46	4	Mesitylene	C9H12
4	7.65	0.62	Carveol	C10H16O
5	8.674	0.73	1-Ethynylcyclododecanol	C14H24O
6	11.735	4.41	Heptadecane	C17H36
7	12.857	4.5	Octadecane	C18H38
8	13.635	3.87	Benzocycloheptatriene	C11H6O
9	14.03	2.73	Benzocycloheptatriene	C11H6O
10	14.957	3.78	Eicosane	C20H42
11	15.06	1.13	Biphenyl	C12H10
12	15.729	0.45	3-(2-Methyl-propenyl)-1H-indene	C13H14
13	15.941	3.44	Heneicosane	C21H44
14	16.107	1.29	1,1'-Biphenyl, 2-methyl-	C13H12
15	16.284	1.02	4,6,8-Trimethylazulene	C13H14
16	16.639	1.09	4,6,8-Trimethylazulene	C13H14
17	17.194	10.46	Hexadecanoic acid, methyl ester	C17H34O2
18	17.24	5.91	Pentadecanoic acid, 14-methyl-, methyl ester	C17H34O2
19	19.483	9.53	Methyl stearate	C19H38O2
20	19.74	13.59	13-Octadecenoic acid, methyl ester	C19H36O2
21	19.792	7.72	13-Octadecenoic acid, methyl ester	C19H36O2
22	19.843	2.33	13-Octadecenoic acid, methyl ester	C19H36O2
23	20.341	15.94	Methyl 9-cis,11-trans-octadecadienoate	C19H34O2

Table 4. Untreated bentonite (B) GC-MS results

Peak	RT	Area (%)	Identified Compounds	Molecular Formula
1	6.12	0.43	Carveol	C10H16O
2	6.326	2.9	Mesitylene	C9H12
3	7.522	0.41	Carveol	C10H16O
4	10.451	3.76	Hexadecane	C16H34
5	11.642	4.09	Heptadecane	C17H36
6	12.271	3.35	Azulene	C10H8
7	12.769	3.79	Octadecane	C18H38
8	13.513	3.25	Benzocycloheptatriene	C11H6O
9	13.845	3.52	Nonadecane	C19H40
10	13.902	2.19	Benzocycloheptatriene	C11H6O
11	14.875	3.39	Eicosane	C20H42
12	14.937	0.98	Biphenyl	C12H10
13	15.613	0.35	3-(2-Methyl-propenyl)-1H-indene	C13H14
14	15.859	3	Heneicosane	C21H44
15	15.99	0.96	1,1'-Biphenyl, 2-methyl-	C13H12
16	16.162	0.83	4,6,8-Trimethylazulene	C13H14
17	16.511	1.1	4,6,8-Trimethylazulene	C13H14
18	17.083	9.51	Pentadecanoic acid, 14-methyl-, methyl ester	C17H34O2
19	17.129	4.23	Pentadecanoic acid, 14-methyl-, methyl ester	C17H34O2
20	17.278	1.48	Azulene, 1,4-dimethyl-7-(1-methylethyl)-	C15H18
21	18.983	2.48	Tetracosane	C24H50
22	19.36	8.08	Methyl stearate	C19H38O2
23	19.607	12.18	13-Octadecenoic acid, methyl ester	C19H36O2
24	19.664	5.89	13-Octadecenoic acid, methyl ester	C19H36O2
25	19.71	1.78	13-Octadecenoic acid, methyl ester	C19H36O2
26	20.207	13.46	Methyl 9-cis,11-trans-octadecadienoate	C19H34O2

Table 5. HCl-bentonite (0.40%) GC-MS results

Peak	RT	Area (%)	Identified Compounds	Molecular Formula
1	1.946	1.14	Dodecane	C12H26
2	2.272	0.61	Dodecane	C12H26
3	2.512	1.22	Dodecane	C12H26
4	3.073	0.83	Dodecane	C12H26
5	6.323	3.01	Mesitylene	C9H12
6	7.525	0.48	Carveol	C10H16O
7	11.639	4.06	Heptadecane	C17H36
8	13.51	3.19	Benzocycloheptatriene	C11H6O
9	13.842	3.43	Nonadecane	C19H40
10	15.616	0.28	3-(2-Methyl-propenyl)-1H-indene	C13H14
11	15.862	2.9	Heneicosane	C21H44
12	16.165	0.93	4,6,8-Trimethylazulene	C13H14
13	16.52	1.03	4,6,8-Trimethylazulene	C13H14
14	17.092	9.25	Hexadecanoic acid, methyl ester	C17H34O2
15	17.132	4.74	Pentadecanoic acid, 14-methyl-, methyl ester	C17H34O2
16	17.281	0.93	Azulene, 1,4-dimethyl-7-(1-methylethyl)-	C15H18
17	19.368	7.86	Methyl stearate	C19H38O2
18	19.621	12.18	13-Octadecenoic acid, methyl ester	C19H36O2
19	19.667	7.38	13-Octadecenoic acid, methyl ester	C19H36O2
20	19.718	1.57	13-Octadecenoic acid, methyl ester	C19H36O2
21	20.216	13.87	Methyl 9-cis,11-trans-octadecadienoate	C19H34O2

Table 6. HCl-bentonite (0.80%) GC-MS results

Peak	RT	Area (%)	Identified Compounds	Molecular Formula
1	6.469	2.98	Mesitylene	C9H12
2	9.731	0.89	2-Pentanone, 4-cyclohexylidene-3,3-diethyl-	C15H26O
3	10.549	3.86	Hexadecane	C16H34
4	11.372	5.82	Pentadecane, 2,6,10,14-tetramethyl-	C19H40
5	11.733	3.76	Heptadecane	C17H36
6	12.403	3.15	Azulene	C10H8
7	12.861	3.57	Octadecane	C18H38
8	13.639	3.18	Benzocycloheptatriene	C11H6O
9	13.931	3.36	Nonadecane	C19H40
10	14.028	2.14	Benzocycloheptatriene	C11H6O
11	14.955	3.14	Eicosane	C20H42
12	15.058	0.91	Biphenyl	C12H10
13	15.727	0.39	3-(2-Methyl-propenyl)-1H-indene	C13H14
14	15.939	2.89	Heneicosane	C21H44
15	16.105	1.08	1,1'-Biphenyl, 2-methyl-	C13H12
16	16.282	1.05	3-(2-Methyl-propenyl)-1H-indene	C13H14
17	16.637	0.91	4,6,8-Trimethylazulene	C13H14
18	17.186	8.3	Pentadecanoic acid, 14-methyl-, methyl ester	C17H34O2
19	17.232	5.08	Pentadecanoic acid, 14-methyl-, methyl ester	C17H34O2
20	17.404	1.37	Azulene, 1,4-dimethyl-7-(1-methylethyl)-	C15H18
21	19.086	2.08	Tetracosane	C24H50
22	19.475	7.82	Methyl stearate	C19H38O2
23	19.733	11.28	13-Octadecenoic acid, methyl ester	C19H36O2
24	19.784	6.18	13-Octadecenoic acid, methyl ester	C19H36O2
25	19.836	1.57	13-Octadecenoic acid, methyl ester	C19H36O2
26	20.334	13.23	Methyl 9-cis,11-trans-octadecadienoate	C19H34O2

generally better than that of oxygen-containing FAME [41]. Therefore, the highest heat value of 42.39 MJ/kg obtained at 0.80% by weight is consistent with GC-MS observations showing the highest fraction of aliphatic hydrocarbons among the nearly complete chromatographic profiles. However, this sample also contains relatively heavy hydrocarbons up to C24. This distribution provides a plausible explanation for why the calorific value increases while viscosity remains relatively high at 4.50 cSt.

This behavior contrasts with that observed at 0.40%. At intermediate catalyst loading levels, the detection of C12 products indicates the formation of a relatively stronger fraction of low-molecular-weight volatiles, consistent with lower viscosity

and flash point. At 0.80%, the product contains a broader distribution of C16–C24 hydrocarbons and a highly branched C19 fraction, resulting in a higher calorific value but a smaller reduction in viscosity. Therefore, the nonlinear trends observed in the physicochemical properties can be explained by differences in product distribution, rather than solely based on the overall FAME conversion rate [19]. Catalyst concentration appears to control not only the extent of transformation but also the molecular weight range of the resulting products.

The aromatic fraction did not show a proportional increase compared to aliphatic hydrocarbons. Aromatic species were already present in the WCO biodiesel and remained detectable after the catalytic treatment. Consequently, their presence cannot be attributed exclusively to catalytic aromatization under the current conditions. Although secondary cyclization, condensation, or aromatization reactions may occur at the acidic catalyst sites, the current GC-MS data are insufficient to quantitatively determine these reaction pathways. Therefore, more convincing evidence of quality improvement lies in the redistribution between FAME and aliphatic hydrocarbons rather than in the formation of aromatic products.

5. Conclusion

This study evaluated the feasibility of mild H_2-free catalytic upgrading of WCO-derived biodiesel using untreated and HCl-activated bentonite at low catalyst loading and a reactor temperature of 150 °C, with the aim of improving the diesel-like fuel properties for direct use in vehicles. This treatment resulted in only negligible changes in density (0.842–0.844 g/cm³), confirming that most of the biodiesel's molecular characteristics were preserved, while the kinematic viscosity decreased substantially from 4.94 cSt to a minimum of 3.54–3.55 cSt at catalyst loadings of 0.20–0.40% by weight. The heat value increased from 41.46 MJ/kg for the initial WCO biodiesel to a maximum of 42.39 MJ/kg at 0.80% by weight, representing an increase of approximately 2.24%, while the 0.60% and 0.80% by weight samples maintained flash points of 57.5 and 56.5 °C, respectively, above the minimum requirements of ASTM D975. Further GC-MS analysis revealed a shift in composition from 65.48% FAME and 16.13% aliphatic hydrocarbons in the initial biodiesel to approximately 53.46% FAME and 28.48% aliphatic hydrocarbons at 0.80% by weight, while the FTIR spectrum confirmed that the dominant ester and long-chain aliphatic functions were largely preserved. The catalyst loading response was clearly nonlinear: intermediate loadings, particularly 0.40% by weight, favored the formation of lighter hydrocarbons such as C12 species and consequently resulted in lower viscosity and flash point, whereas 0.80% by weight promoted a broader distribution of C16–C24 hydrocarbons, thereby increasing the calorific value but yielding a smaller reduction in viscosity. These findings indicate that catalyst concentration controls not only the degree of transformation but also the molecular weight distribution of the products, suggesting that mild enhancement can improve specific fuel properties without requiring deep conversion characteristics such as conventional cracking or hydrodeoxygenation. However, since direct measurements of oxygen content, detailed structural/acidity characterization of the catalyst, and replication-based statistical analysis are not available, future research should measure oxygen removal, characterize the catalyst's active sites, and systematically optimize catalyst loading, reaction time, and temperature to determine the relationship between catalyst properties, reaction pathways, and long-term fuel performance.

6. Limitation

This study is limited by the absence of direct oxygen-content and CHNS/O elemental analyses, acid-number measurements, complete mass-balance data, detailed catalyst structural and acidity characterization, and replicate-based statistical evaluation. In addition, because untreated bentonite was evaluated only at 0.2 wt%, the effects of acid activation could not be independently distinguished from catalyst-loading effects across the entire concentration range. Future studies should therefore incorporate quantitative oxygen analysis, catalyst characterization, complete product mass balances, replicate experiments, and matched untreated/activated catalyst loadings to clarify the underlying reaction pathways and confirm the extent of catalytic transformation.

Acknowledgements

The authors gratefully acknowledge financial support from the Ministry of Higher Education, Science, and Technology of the Republic of Indonesia (Kemdiktisaintek) under the PMDSU program with grant number: 064/C3/DT.05.00/PL/2025 and 642/UN10.A0501/B/PT.01.03.2/2025.

Author's Declaration

Authors' contributions and responsibilities

M.L.R.: Conceptualization, Methodology, Data curation, Validation. N.H.: Supervision, Conceptualization, Methodology, Data curation, Validation. W.: Supervision, Conceptualization, Methodology, Data curation, Validation.

Funding

Ministry of Higher Education, Science, and Technology of the Republic of Indonesia (Kemdiktisaintek) under the PMDSU program with grant number: 064/C3/DT.05.00/PL/2025 and 642/UN10.A0501/B/PT.01.03.2/2025.

Availability of data and materials

All data are available from the authors.

Competing interests

The authors declare no competing interest.

Generative AI statement

The authors used ChatGPT (OpenAI) to assist with language refinement and manuscript preparation. All AI-generated outputs were carefully reviewed, verified, and revised by the authors to ensure their accuracy and scientific validity. The authors take full responsibility for the content of the final manuscript.

Additional information

No additional information from the authors.

References

[1] N. Ilminnafik, D. H. T. Prasetiyo, Welayaturromadhona, A. M. Kartini, B. Palupi, and Suyitno, "Optimization of biodiesel synthesis process from nyamplung (calophyllum inophyllum) oil using thermal air sparging method," *Mechanical Engineering for Society and Industry*, vol. 6, no. 1, May 2026, doi: 10.31603/mesi.15335.

[2] S. Devasthali, A. Kulkarni, N. Bhatkar, and U. Sankpal, "Metal Oxide Doped Egg Shell-Fly Ash Composite: An Effective Catalyst for Transesterification of Waste Oil," *ECS Transactions*, vol. 107, no. 1, pp. 13103–13112, Apr. 2022, doi: 10.1149/10701.13103ecst.

[3] R. C. Nnamani, P. N. Okwu, B. John, and O. J. Abayeh, "Preliminary Investigation of Transesterified Waste Cooking Oil (WCO) as a Biodiesel," *Journal of Chemical Society of Nigeria*, vol. 45, no. 5, 2020, doi: 10.46602/jcsn.v45i5.515.

[4] A. Kolakoti, M. Setiyo, and B. Waluyo, "Biodiesel Production from Waste Cooking Oil: Characterization, Modeling and Optimization," *Mechanical Engineering for Society and Industry*, vol. 1, no. 1, pp. 22–30, Jul. 2021, doi: 10.31603/mesi.5320.

[5] A. B. Pratama, S. M. Benu, E. P. D. Boangmanalu, S. Siahaan, and H. Ibrahim, "Analisis Laju Korosi Baja Karbon Ringan pada Biopelumas dari Limbah Minyak Goreng," *SINERGI POLMED: Jurnal Ilmiah Teknik Mesin*, vol. 6, no. 1, pp. 7–18, Mar. 2025, doi: 10.51510/sinergipolmed.v6i1.1933.

[6] S. M. Benu, E. P. D. Boangmanalu, A. B. Pratama, and M. A. Pulungan, "Sintesis Pelumas Biodegradable dari Limbah Minyak Goreng Melalui Pendekatan Respon Permukaan," *SINERGI POLMED: Jurnal Ilmiah Teknik Mesin*, vol. 6, no. 1, pp. 19–27, Mar. 2025, doi: 10.51510/sinergipolmed.v6i1.1934.

[7] S. Suherman *et al.*, "A Review of Properties, Engine Performance, Emission Characteristics and Material Compatibility Biodiesel From Waste Cooking Oil (WCO)," *Automotive Experiences*, vol. 6, no. 3, pp. 624–651, Nov. 2023, doi: 10.31603/ae.10128.

[8] S. Suherman, M. Muharnif, I. Abdullah, A. S. Silitonga, M. Yusfiani, and W. A. W. Hamzah, "Two Decades of Biodiesel Research from Waste Cooking Oil: A Bibliometric and Literature Review of Heterogeneous Catalysts," *Automotive Experiences*, vol. 8, no. 3, pp. 573–598, Dec. 2025, doi: 10.31603/ae.14776.

[9] D. Darwin, R. A. M. Harahap, A. Pratama, M. Thifa, and M. A. Alwi Fayed, "Enhanced biodiesel production from waste cooking oils catalyzed by sodium hydroxide supported on heterogeneous co-catalyst of bentonite clay," *Research in Agricultural Engineering*, vol. 69, no. 3, pp. 124–131, Sep. 2023, doi: 10.17221/70/2022-RAE.

[10] K. Maqsood and M. Alsaady, "Optimization

using response surface methodology for producing biodiesel from waste cooking oil using fishbone catalyst," *Materialwissenschaft und Werkstofftechnik*, vol. 53, no. 10, pp. 1242–1248, Oct. 2022, doi: 10.1002/mawe.202200138.

[11] Y. Zetra *et al.*, "Synthesis of 2-Hidroxyethyl Ester (2-HEE) and 2-Hydroxypropyl Ester (2-HPE) from Castor Oil as Bioadditives to Improve the Cold Flow Characteristic of Biodiesel," *Automotive Experiences*, vol. 9, no. 1, May 2026, doi: 10.31603/ae.15860.

[12] J. Milano *et al.*, "Tribological study on the biodiesel produced from waste cooking oil, waste cooking oil blend with Calophyllum inophyllum and its diesel blends on lubricant oil," *Energy Reports*, vol. 8, pp. 1578–1590, Nov. 2022, doi: 10.1016/j.egyr.2021.12.059.

[13] V. G. Nguyen, M. T. Pham, N. V. L. Le, H. C. Le, T. H. Truong, and D. N. Cao, "A comprehensive review on the use of biodiesel for diesel engines," *International Journal of Renewable Energy Development*, vol. 12, no. 4, pp. 720–740, Jul. 2023, doi: 10.14710/ijred.2023.54612.

[14] E. Demir, S. D. Çalhan, and Ö. Sönmez, "Microwave-assisted biodiesel production from waste cooking oil using deep eutectic solvent catalyst: Kinetic and thermodynamic insights," *Biomass and Bioenergy*, vol. 201, p. 108148, Oct. 2025, doi: 10.1016/j.biombioe.2025.108148.

[15] M. Karthikeyan, S. Sathish, M. R. Soosai, D. Prabu, and D. Venkatesan, "Optimized production of biodiesel from used (waste) cooking oil by utilizing a heterogeneous catalyst, and its studies for sustainable development," *Fuel*, vol. 403, p. 136091, Jan. 2026, doi: 10.1016/j.fuel.2025.136091.

[16] A. Kolakoti, M. Setiyo, and M. L. Rochman, "A Green Heterogeneous Catalyst Production and Characterization for Biodiesel Production using RSM and ANN Approach," *International Journal of Renewable Energy Development*, vol. 11, no. 3, pp. 703–712, 2022, doi: 10.14710/ijred.2022.43627.

[17] S. O. Effiom *et al.*, "Cost, Emission, and Thermo-Physical Determination of Heterogeneous Biodiesel from Palm Kernel Shell Oil: Optimization of Tropical Egg Shell Catalyst," *Indonesian Journal of Science and Technology*, vol. 9, no. 1, pp. 1–32, Nov. 2023, doi: 10.17509/ijost.v9i1.64006.

[18] N. A. A. Rahman, F. Cardenas-Lizana, and A. Sanna, "Lithium–Sodium Fly Ash-Derived Catalyst for the In Situ Partial Deoxygenation of Isochrysis sp. Microalgae Bio-Oil," *Catalysts*, vol. 13, no. 7, p. 1122, Jul. 2023, doi: 10.3390/catal13071122.

[19] T. Maluangnont, P. Praserthdam, and T. Sooknoi, "Catalytic deoxygenation of fatty acids via ketonization and α-carbon scissions over layered alkali titanate catalysts under N 2," *RSC Advances*, vol. 12, no. 53, pp. 34293–34302, 2022, doi: 10.1039/D2RA06530D.

[20] W. He *et al.*, "Synthesis of Chainlike ZSM-5 with a Polyelectrolyte as a Second Template for Oleic Acid and Ethanol Cracking into Light Olefins," *ACS Omega*, vol. 7, no. 44, pp. 40520–40531, Nov. 2022, doi: 10.1021/acsomega.2c05763.

[21] F. P. de Sousa, G. P. dos Reis, and V. M. D. Pasa, "Catalytic pyrolysis of vegetable oils over NbOPO4 for SAF and green diesel production," *Journal of Analytical and Applied Pyrolysis*, vol. 177, p. 106314, Jan. 2024, doi: 10.1016/j.jaap.2023.106314.

[22] F. Shi *et al.*, "Green diesel-like hydrocarbon production by H2-free catalytic deoxygenation of oleic acid via Ni/MgO-Al2O3 catalysts: Effect of the metal loading amount," *Journal of Environmental Chemical Engineering*, vol. 11, no. 5, 2023, doi: 10.1016/j.jece.2023.110520.

[23] Y. Buyang *et al.*, "Dolomite catalyst for fast pyrolysis of waste cooking oil into hydrocarbon fuel," *South African Journal of Chemical Engineering*, vol. 45, pp. 60–72, Jul. 2023, doi: 10.1016/j.sajce.2023.04.007.

[24] B. F. H. de Oliveira, B. M. Viegas, M. Velasquez, and E. N. Macêdo, "Sustainable Valorization of Palm Fatty Acid Distillate into Green Diesel Using Ni–Co Catalysts Supported on Zeolite from Kaolin Waste under Solvent- and Hydrogen-Free Conditions," *ACS Omega*, vol. 10, no. 45, pp. 54967–54977, Nov. 2025, doi: 10.1021/acsomega.5c08463.

[25] R. khan, S. Kaithwas, P. Choudhary, R. Anant, and S. H. Dhawane, "Synergistic

thermocatalytic cracking and in-situ hydrogenation of waste cooking oil for co-production of sustainable aviation fuel and clean hydrogen," *International Journal of Hydrogen Energy*, vol. 191, p. 152189, Nov. 2025, doi: 10.1016/j.ijhydene.2025.152189.

[26] K. B. Tan *et al.*, "Catalytic deoxygenation of stearic acid into olefins over Pt catalysts supported on MOF-derived metal oxides," *Catalysis Science & Technology*, vol. 14, no. 12, pp. 3436–3447, 2024, doi: 10.1039/D4CY00189C.

[27] K. R. Rao, R. B. Pace, H. Suarez, E. Santillan-Jimenez, and C. Risko, "Carboxylic Acid Decarbonylation on Nickel: The Critical Role of the Acid Binding Geometry," *ACS Catalysis*, vol. 13, no. 13, pp. 9102–9112, Jul. 2023, doi: 10.1021/acscatal.3c01489.

[28] R. Wei *et al.*, "Hydrodeoxygenation of oleic acid over NiCu bimetallic catalysts supported on Mo-modified niobium phosphate," *New Journal of Chemistry*, vol. 49, no. 12, pp. 4849–4859, 2025, doi: 10.1039/D4NJ04885G.

[29] E. O. Schipanskaya *et al.*, "Catalytic Biomass Transformation to Hydrocarbons under Supercritical Conditions over Nickel Supported on Schungite," *Processes*, vol. 12, no. 7, p. 1503, Jul. 2024, doi: 10.3390/pr12071503.

[30] M. Slezáčková, A. Peller, J. Mikulec, M. Banič, J. Blaško, and E. Hájeková, "Catalytic hydroprocessing of camelina oil/AGO mixtures over NiMoP/γ-Al2O3 catalysts," *Catalysis Today*, vol. 423, p. 113953, Nov. 2023, doi: 10.1016/j.cattod.2022.11.014.

[31] A. I. Tsiotsias *et al.*, "Selective catalytic deoxygenation of palm oil to produce green diesel over Ni catalysts supported on ZrO2 and CeO2–ZrO2: Experimental and process simulation modelling studies," *Renewable Energy*, vol. 206, pp. 582–596, Apr. 2023, doi: 10.1016/j.renene.2023.02.038.

[32] M. Lalitpattarakit *et al.*, "Effects of operating parameters on green diesel production via deoxygenation of triglycerides," *Chemical Engineering Journal*, vol. 508, 2025, doi: 10.1016/j.cej.2025.161125.

[33] K. Wu *et al.*, "In-situ preparation of MnFeCoNiCu/C for the sustainable co-production of bio-jet fuel and green diesel under solvent-free and low hydrogen pressure conditions," *Energy Conversion and Management*, vol. 318, p. 118875, Oct. 2024, doi: 10.1016/j.enconman.2024.118875.

[34] S. Palanisamy and K. Kandasamy, "Direct Hydrogenation and Hydrotreating of Neat Vegetal Oil into Renewable Diesel Using Alumina Binder with Zeolite," *Revista de Chimie*, vol. 71, no. 9, pp. 98–112, Sep. 2020, doi: 10.37358/RC.20.9.8321.

[35] C. Jia, C. Zhang, S. Xie, W. Zhang, Z. Wang, and H. Lin, "One-pot production of jet fuels from fatty acids and vegetable oils in biphasic tandem catalytic process," *Fuel*, vol. 302, p. 121060, Oct. 2021, doi: 10.1016/j.fuel.2021.121060.

[36] X. Wang *et al.*, "Catalytic pyrolysis of microalgal lipids to liquid biofuels: Metal oxide doped catalysts with hierarchically porous structure and their performance," *Renewable Energy*, vol. 212, pp. 887–896, Aug. 2023, doi: 10.1016/j.renene.2023.05.119.

[37] H. Saad, T. Turki, M. Mezni, S. Sellimi, A. Garbout, and E. Srasra, "Acid-activated clay-polyphenols hybrids from pomegranate peel waste: Towards multifunctional optical and antioxidant materials," *Chemical Physics Impact*, vol. 12, p. 101000, Jun. 2026, doi: 10.1016/j.chphi.2026.101000.

[38] W. Wahyudi, M. Nadjib, and A. Faizi, "Physical property analysis of biodiesel from nyamplung and used cooking oil: density, viscosity, calorific value, and flash point," *Jurnal Polimesin*, vol. 22, no. 2, p. 206, Apr. 2024, doi: 10.30811/jpl.v22i2.4565.

[39] S. Thanikodi, S. Rathinasamy, J. Giri, A. K. Jagadeesan, and E. Makki, "Biodiesel Production from Food Industrial Waste of Soybean Oil using a Lipase-nanoparticle Bio-composite Catalyst," *Automotive Experiences*, vol. 7, no. 2, pp. 189–206, Aug. 2024, doi: 10.31603/ae.10707.

[40] B. O. Yusuf, S. A. Ganiyu, A. M. P. Peedikakkal, and S. A. Oladepo, "ZnO/Cu-BTC metal-organic frameworks as a heterogeneous catalyst for efficient transformation of waste cooking oil into biodiesel," *Biomass and Bioenergy*, vol. 204, p. 108381, Jan. 2026, doi:

10.1016/j.biombioe.2025.108381.

[41] K. Yadav, S. Almansour, L. M. Alkwai, A. Yadav, and F. Ranjbar, "Reliable models for density in waste cooking oil biodiesel-alcohol mixtures using advanced learning techniques," *Industrial Crops and Products*, vol. 234, p. 121602, Oct. 2025, doi: 10.1016/j.indcrop.2025.121602.

[42] J. Guo *et al.*, "Kinetic Evidence of Most Abundant Surface Intermediates Variation over Pt n and Pt p : Few-Atom Pt Ensembles Enable Efficient Catalytic Cyclohexane Dehydrogenation for Hydrogen Production-II," *ACS Catalysis*, vol. 12, no. 12, pp. 7248–7261, Jun. 2022, doi: 10.1021/acscatal.2c01420.

[43] M. L. Rochman, N. Hamidi, F. Gapsari, and W. Winarto, "Green diesel and its role as a drop-in renewable diesel alternative to FAME-based biodiesel," *Mechanical Engineering for Society and Industry*, vol. 5, no. 2, pp. 288–291, Jan. 2026, doi: 10.31603/mesi.13658.

[44] J. Fu, "Flash points measurements and prediction of biofuels and biofuel blends with aromatic fluids," *Fuel*, vol. 241, pp. 892–900, 2019, doi: 10.1016/j.fuel.2018.12.105.

[45] M. H. Al-Abdullah, G. T. Kalghatgi, and H. Babiker, "Flash points and volatility characteristics of gasoline/diesel blends," *Fuel*, vol. 153, pp. 67–69, 2015, doi: 10.1016/j.fuel.2015.02.070.

[46] J. M. Da Costa *et al.*, "Characterization of Biodiesel from Animal Fat, Vegetable Oil, and Adulterants by Infrared Spectroscopy Combined with Chemometric Methods," *Energy and Fuels*, vol. 35, no. 17, pp. 13801–13812, 2021, doi: 10.1021/acs.energyfuels.1c00911.

[47] I. C. Castellanos Cuellar, E. Avella-Moreno, P. M. Vargas-Molina, and A. M. Bejarano, "An Interference Free Absorption In The Mid-Infrared to Follow the Obtaining of Biodiesel by Transesterification of Waste Frying Oils," *Momento*, vol. 2023, no. 67, pp. 39–54, Jul. 2023, doi: 10.15446/mo.n67.107249.

[48] V. Sathiyaseelan, S. Chinnasamy, V. D. Tamilarasan, A. Sampathkumar, M. Manikandan, and S. Veeraraghavan, "Comprehensive Spectroscopic and Chromatographic Analysis of Waste Fish Oil Biodiesel using NMR, GC-MS, and FTIR Techniques for Sustainable Alternative Fuel Production," *Malaysian Journal of Chemistry*, vol. 27, no. 3, pp. 370–390, 2025, doi: 10.55373/mjchem.v27i3.370.

[49] M. Ahda, A. Guntarti, A. Kusbandari, and A. Safitri, "Identification of Lard Adulteration of Cooking Oil Products Using Fourier Transform Infrared Spectroscopy Combined with Chemometrics," *Food Analytical Methods*, vol. 17, no. 3, pp. 366–372, 2024, doi: 10.1007/s12161-024-02576-y.

[50] W. Du *et al.*, "Combined determination analysis of surface properties evolution towards bentonite by pH treatments," *Colloids and Surfaces A: Physicochemical and Engineering Aspects*, vol. 626, p. 127067, Oct. 2021, doi: 10.1016/j.colsurfa.2021.127067.